Journal of Materials Chemistry B

ROYAL SOCIETY OF CHEMISTRY

PAPER

View Article Online
View Journal

Cite this: DOI: 10.1039/d5tb01033k

Encapsidic production and isolation of degradation-prone polypeptides

Agnieszka Gawin, [a] Jedrzej Pankowski, †[ab] Maria Zarechyntsava, †[ab] Dominika Kwasna, [a] Damian Kloska, [a] Lukasz Koziej, [a] Sebastian Glatt, [ac] Neli Kachamakova-Trojanowska [a] and Yusuke Azuma *[a]

Received 30th April 2025,
Accepted 22nd August 2025

DOI: 10.1039/d5tb01033k

rsc.li/materials-b

Degradation during production and delivery is a significant bottleneck in developing biomolecular therapies. Protein cages, formed by engineered variants of lumazine synthase, present an effective strategy for the microbial production and isolation of labile biomolecular therapies. Genetic fusion of the target polypeptide to a cage component protomer ensures its efficient encapsulation within the cage during production in host bacterial cells, thereby protecting it from degradation. Furthermore, controlled cage opening outside the cellular environment facilitates the isolation of the encapsulated cargo through sequence-specific protease cleavage. Notably, the system features a modular patchwork assembly to prevent guest overloading, avoiding unwanted incomplete cage formation and insoluble aggregates. The broad applicability of the "encapsidic" approach is demonstrated by the efficient production of six distinct, intrinsically disordered polypeptides with proven therapeutic potential.

Introduction

Encapsulation in hollow proteinaceous compartments is a common biological strategy for the protective storage and delivery of otherwise unstable substances. Spatial segregation by a physical barrier circumvents unwanted chemical transformation of cargoes, and their specialized release mechanism liberates them at the desired timing and location. For instance, viruses use capsids for protectively packaging their genomic materials and delivering them to the next host cells.[1–3] Ferritin stores iron ions in the lumen while preventing the production of toxic reactive oxygen species and releases them when needed.[4] These naturally occurring protein cages not only provide inspiration but also "almost-ready-to-use" platforms for developing customized nanometric molecular carriers.[5,6]

Engineered protein cages have been exploited for both intra- and extracellular delivery routes. The majority of the current research seeks to load protein cages with molecules of interest outside the biological context to deliver the guest cargo into cells.[7] In the opposite scenario, protein cages can capture target molecules while being produced in host cells and transport them outside of the cells. For instance, viral capsids and their mimicries have been shown to package target RNA within cells and protect them from nucleases and other processing enzymes.[8–12] Such a protective storage function highlights the potential of protein cages as powerful tools for the intracellular production of valuable molecules that are otherwise rapidly degraded or converted by intracellular machinery.

Protein cages can protect encapsulated cargo proteins from degradation by cellular proteases. This has been demonstrated with cargo proteins carrying a degradation sequence in combination with a localization signal.[13–18] While the degron tag would trigger the rapid proteolysis, encapsulation in protein shells mediated by the localization peptide prevents the degradation process by shielding cargoes from the proteolytic machinery. We have described such a rescue effect for engineered variants of a cage-forming lumazine synthase from *Aquifex aeolicus* (AaLS), where the negatively charged lumen of the shell-like structure protectively encapsulates a positively supercharged green fluorescent protein, GFP(+36), fused to a bacterial degradation tag.[19] However, in these previous studies, degradation signals were used to assess cargo encapsulation in the intracellular environment, and major questions and concerns have remained about the practicability of protein cages for heterologous protein production and isolation. Here, we report that an AaLS-based cargo encapsulation system offers a simple and robust solution for producing otherwise degradation-prone polypeptides in bacterial cells and their efficient isolation outside cellular contexts.

[a] *Malopolska Centre of Biotechnology, Jagiellonian University, Krakow 30-387, Poland. E-mail: yusuke.azuma@edu.uj.pl*
[b] *Faculty of Biochemistry, Biophysics, and Biotechnology, Jagiellonian University, Krakow 30-387, Poland*
[c] *Department for Biological Sciences and Pathobiology, University of Veterinary Medicine Vienna, 1210 Vienna, Austria*
† These authors contributed equally to this work and are listed alphabetically.

Results and discussion

Rescue of degradation-prone GFP by encapsulation in AaLS cages

We previously established a robust protein encapsulation system using a circularly permuted variant of AaLS (cpAaLS),[20]

which positions the N- and C-termini pointing towards the cage interior. In this system, a protein of interest is genetically fused to cpAaLS and simultaneously produced with an excess of another AaLS variant, such as wildtype AaLS (AaLS-wt), in *Escherichia coli* cells (Fig. 1a). Coassembly of these AaLS proteins allows the formation of cage-like structures encapsulating the fusion partner in the lumen. The intracellular production level of these constituent proteins can be regulated individually by tetracycline or isopropyl-β-D-thiogalactopyranoside (IPTG). This is crucial to avoid excessive cargo loading that inhibits cage assembly due to steric hindrance.[20] This simple and modular compartmentalization system represents an ideal platform for exploring the potential of protein cages to produce degradation-prone proteins and peptides within cells. We refer to this heterologous protein production in capsid-like protein shells as ''encapsidic'' production.

AaLS protein is known to adopt a variety of assembly statuses upon mutagenesis,[10,21–23] and the variant that predominantly constitutes patchwork cages rules the entire morphology.[8,20] While the wildtype protein forms ~16-nm dodecahedral structures composed of 12 copies of pentameric subunits (Fig. 1b, left),[24] the negatively supercharged variants, AaLS-neg and AaLS-13, assemble into expanded ~28-nm and ~40-nm particles composed of 36 and 72 pentamers, respectively.[21] When cpAaLS is coproduced with excess AaLS-wt, AaLS-neg, or AaLS-13, the morphology of the resulting patchwork structures resembles those formed by the latter AaLS variants alone.[20] In this study, we used AaLS-wt or a cpAaLS derivative possessing a His-tag in the linker connecting native termini (cpAaLS(His))[20] as a scaffold protein to form patchwork cages. This cpAaLS(His) variant assembles into ~24-nm and ~28-nm hollow particles[20] composed of 24- or 36-pentameric subunits, respectively. Notably, these expanded cage-like structures have large ~4 nm keyhole-shaped pores in the walls (Fig. 1b, middle and right).[22] These AaLS variants with distinct assembly characteristics allow us to investigate the impact of the morphological features on the protection of encapsulated cargoes.

As a model of a degradation-prone cargo protein, we primarily employed a destabilized variant of GFP.[19] This variant possesses a bacterial signal peptide, SsrA,[25] which triggers the degradation of the fusion partner by the housekeeping proteases ClpXP and ClpAP.[26] When GFP fused to the SsrA tag (GFP-SsrA) is produced in *Escherichia coli* cells, the intracellular concentration of the protein remains low due to its rapid proteolysis. This expected effect was confirmed by flow cytometry analysis of *E. coli* producing GFP-SsrA and GFP without the tag (Fig. S1).

Encapsulation in protein cages should avoid a destined degradation of SsrA-tagged proteins by preventing their access to the proteolytic machinery.[19] To test this, GFP-SsrA was fused to the C-terminus of cpAaLS (cpAaLS-GFP-SsrA) and produced in *E. coli*. Notably, this fusion variant itself is unable to form an intact cage-like structure due to the steric hindrance of cargo GFP (Fig. 2a).[20] Indeed, flow cytometry analysis of cells producing cpAaLS-GFP-SsrA showed that the fluorescence intensity is comparable to that of background autofluorescence (Fig. 2b and c, dark red and grey), indicating rapid degradation. However, coproduction of cpAaLS-GFP-SsrA with AaLS-wt or cpAaLS(His) increased the mean fluorescence intensity 73 or 63 times, respectively (Fig. 2b and c, blue and orange), suggesting protective guest encapsulation for both combinations. Of note, these fluorescent values correspond to approximately 60% or 50% of the respective signals observed with cpAaLS-GFP lacking the SsrA tag (Fig. 2b and c, red, orange, and blue). These rescue effects are significantly higher in comparison to a complimentary charge-driven encapsulation system we previously investigated.[19] Compared to reversible, non-covalent interaction, genetic fusion to a cage component protein probably yields a kinetic advantage for reducing cargo release and exposure to cellular proteases, resulting in increased levels of cargo protection.

The AaLS-wt and cpAaLS(His) proteins coproduced with cpAaLS-GFP-SsrA were isolated using affinity chromatography and characterized outside cells (Fig. 2c–e). Negative-stain

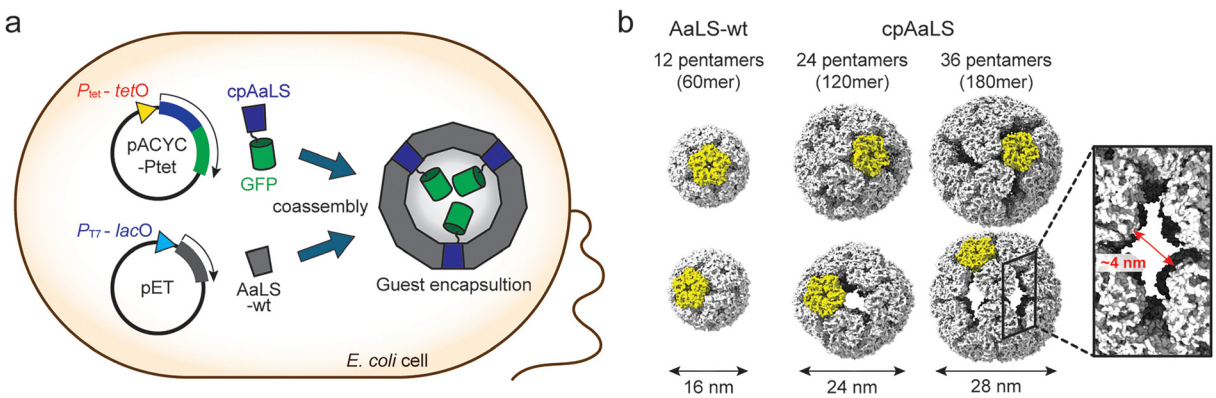

Fig. 1 Guest encapsulation in AaLS cages using genetic fusion and patchwork assembly. (a) Schematic representation of the guest encapsulation. Coproduction of guest protein, *e.g.*, GFP, fused to cpAaLS with another AaLS protein, *e.g.*, AaLS-wt, in *E. coli* cells, leads to simultaneous coassembly and guest encapsulation in patchwork cages. Expression of the genes encoding these proteins is regulated individually by the tetracycline promoter combined with the tetracycline operator (P_{tet} – *tetO*) or the T7 promoter combined with the lactose operator (P_{T7} – *lacO*), respectively. (b) Structures of AaLS-wt (PDB ID: 1HQK) and cpAaLS (9G3O and 9G3N) assemblies. These cages are shown from two different viewing angles, and a representative pentamer unit is highlighted in yellow. Both cpAaLS assemblies have large keyhole-shaped pores in the wall, shown in a cropped and enlarged image.

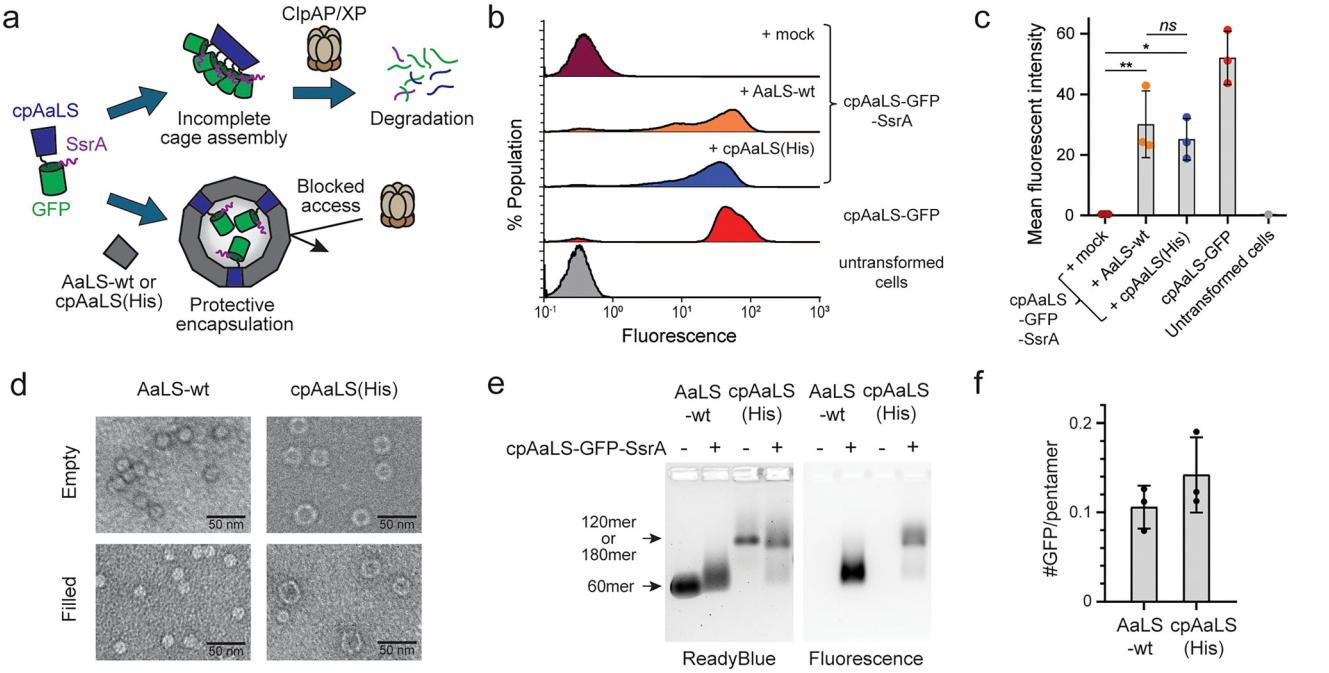

Fig. 2 Protective encapsulation of a degradation-prone GFP variant. (a) Conceptual scheme of protective encapsulation of GFP equipped with a bacterial degradation tag SsrA (GFP-SsrA). When cpAaLS-GFP-SsrA is produced alone, cage assembly is hindered by guest steric repulsion, resulting in exposure of the SsrA tag and degradation by ClpAP/XP proteases. Patchwork coassembly with AaLS-wt or cpAaLS(His) proteins allows intact cage formation and guest protection. (b) Histogram representing fluorescence intensity within populations of cells coproducing cpAaLS-GFP-SsrA with either AaLS-wt (orange) or cpAaLS(His) (blue). The results from cells producing cpAaLS-GFP-SsrA with the mock plasmid (dark red), cpAaLS-GFP (red), and untransformed cells are also provided for comparison. 100% population corresponds to the total number of the analyzed cells (*Y*-axis scale, 0–1.2%). (c) Mean fluorescence intensity of the flow cytometry experiments. (d) and (e) Negative-stain transmission electron microscopy (TEM) images (d) and native-agarose gel electrophoresis (e) of AaLS-wt and cpAaLS(His) coproduced with cpAaLS-GFP-SsrA. The bands in the gel are visualized with ReadyBlue staining (left) and fluorescent staining (right). The corresponding AaLS cages without cargo GFP are provided as the gel mobility standard, and the bands are marked by arrows. (f) Quantification of the number of GFP per pentamer. For panels c and f, data are shown as means ± standard deviation from three biological replicates. ns – $p > 0.05$; * – $p < 0.1$; ** – $p < 0.01$ (one-way ANOVA with Dunnett's test).

transmission electron microscopy (TEM) and native agarose gel electrophoresis (AGE) of the AaLS-wt sample confirmed successful complex formation with cpAaLS-GFP-SsrA resembling the observed morphology of the cages without cargo (Fig. 2d and e). Efficient complex formation was also observed with cpAaLS(His) coproduced with cpAaLS-GFP-SsrA, where most of the particles were confirmed to be ~24- or ~28-nm spheres, but a small fraction of the wildtype-like ~16-nm particles, that were absent with cpAaLS(His) alone, could also be detected (Fig. 2d and e). Encapsulated GFP-SsrA and associated impurities (Fig. S2) possibly have an effect on the cpAaLS(His) assemblies. The number of GFP per AaLS-wt 60mer or cpAaLS(His) 180mer cage was estimated by the absorbance ratio at 280/475 nm as 1.3 and 5.1, corresponding to 0.11 and 0.14 GFP molecules per pentamer, respectively (Fig. 2f).[22,27] Together with the presented flow cytometry experiments, these results confirm little difference between the AaLS-wt and cpAaLS(His) cages, despite the distinct porosity in the walls, in protective guest encapsulation of the SsrA-tagged proteins.

Cargo GFP retrieval by protease cleavage

Upon successfully protecting the degradation-prone GFP variant from cellular proteases, we next sought to retrieve the cargo proteins from the AaLS cages and redesigned the protein constructs accordingly. First, a recognition sequence for the commonly used tobacco etch virus (TEV) protease[28–30] was introduced between cpAaLS and GFP-SsrA, yielding cpAaLS-tev*-GFP-SsrA (Fig. 3a), so that the cargo proteins can be disconnected from the cage-forming protomers by proteolytic cleavage. Additionally, the His-tag region of AaLS(His) was replaced by a Strep II tag as nickel-based affinity chromatography remains a concern for purifying therapeutic biomolecules due to the potential contamination of toxic metal ions (Table S1). This variant, called cpAaLS(Strep), was produced as a mixture of 24- and 28-nm spherical assemblies, like the parent cpAaLS(His) (Fig. S3). Notably, this tag replacement and the change in the affinity chromatography method resulted in a significantly improved purification yield: ~1 mg cpAaLS(His) and ~15 mg cpAaLS(Strep) from *E. coli* cell culture in a 0.25-L Luria–Bertani (LB) medium.

TEV protease (~3.5 nm) is smaller than the pores (~4 nm) of cpAaLS assemblies (Fig. 1b). Therefore, we assumed the enzyme would be able to enter the inner cavity of the protein cages and release the cargo GFP by proteolytic digest (Fig. 3b), while this would not occur with the AaLS-wt cages possessing only small (~3 Å) pores (Fig. 1b). To verify this hypothesis, AaLS-wt and cpAaLS(Strep) patchwork assemblies containing cpAaLS-tev*-GFP-SsrA were treated with an engineered variant of TEV proteases,[28–30] and the cleavage was monitored by SDS-

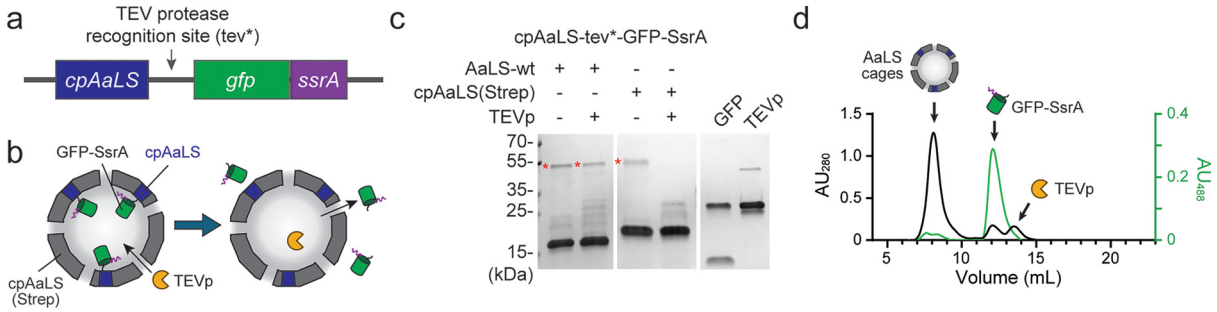

Fig. 3 GFP retrieval from AaLS cages. (a) Design of cpAaLS fusion to GFP-SsrA *via* the TEV protease recognition site (tev*). (b) Hypothetical mechanisms of TEV protease (TEVp) entry into cpAaLS(Strep) cages through the ~4-nm pores and resulting GFP release. (c) SDS-PAGE analysis of the cleavage reaction. Red asterisks indicate the bands corresponding to cpAaLS-tev*-GFP-ssrA (47.6 kDa). The theoretical molecular masses of other proteins are as follows: AaLS-wt, 18.1 kDa; cpAaLS(Step), 18.5 kDa; TEVp, 28.8 kDa; and GFP-SsrA, 29.1 kDa. The bands for TEVp and GFP-SsrA are undistinguishable due to the minor differences in their molecular masses. (d) Size-exclusion chromatography confirming that GFP-SsrA is released from the cpAaLS cages upon cleavage, shown as absorbance at 280 nm (black) and 488 nm (green). AaLS cages were eluted at the void volume (7–8 mL) of a Superdex 75 column.

PAGE (Fig. 3c). Unexpectedly, the proteolytic reaction was observed for the cages based on AaLS-wt, albeit at a low efficiency of ~30%. This partial cleavage might result from imperfectly assembled AaLS-wt cages, possibly due to overloading by cargo. Strikingly, the cleavage efficiency for patchwork cages based on cpAaLS(Strep) was almost complete. These results underline that cage-like assemblies with large pores enable the TEV protease to enter the protein cages and cleave the cargo at the specific recognition motif (Fig. 3b). This cleavage does not lead to a noticeable morphology change for either type of AaLS cages, as judged by the TEM images (Fig. S4). Size-exclusion chromatography (SEC) confirmed that the cleaved GFP was indeed released from the still intact host cages (Fig. 3d).

The keyhole-shaped, ~4-nm dimension pores of cpAaLS(-Strep) cages likely allow passage of smaller molecules (Fig. 1 and Fig. S5a). This is advantageous for guest retrieval using a sequence-specific protease such as TEV protease and guest release upon cleavage *in vitro*. At the same time, this porous shell still serves as a barrier to prevent the internalization of major proteolytic machinery in bacterial cells such as ClpXP or FtsH that are much larger (~16 nm) or are membrane-bound (Fig. S5b).[31] Therefore, the porous nature of cpAaLS(Strep) cages appears to provide an ideal system for microbial production of degradation-prone proteins and their retrieval outside cellular contexts.

Encapsidic production of a glucagon-like peptide 1 derivative, lixisenatide

Beyond the SsrA-based proof-of-concept model, we envisaged that the encapsidic production system would be useful for clinically relevant bioactive molecules. Along this line, we focused on short, intrinsically disordered peptides that are typically difficult to produce recombinantly due to the rapid degradation by endogenous proteases in host cells.[32,33] The current peptide production largely relies on chemical synthesis, which requires excess molarity of expensive and harmful reactants and, therefore, remains a concern in cost and waste management.[34] Furthermore, synthesizing relatively long peptides, >40 residues, is often burdensome, whereas amino acid length is ultimately not a limiting factor in recombinant protein production. Given the remarkable progress in peptide therapeutic development in the last decade and its increasing global market,[35,36] there is a need for an inexpensive and ecological platform for their production, where the microbe-based encapsidic production system potentially meets the criteria.

As an initial model of therapeutic peptides, we selected a glucagon-like peptide 1 (GLP-1) derivative, lixisenatide (LIX), an antidiabetic drug composed of 44 amino acids (Table S2).[37] This peptide was fused to the C-terminus of cpAaLS *via* a TEV protease recognition site, referred to as cpAaLS-tev*-LIX, and coproduced with cpAaLS(His) or cpAaLS(Strep) (Fig. 4a, patchwork cage). Additionally, we tested a sole production of cpAaLS(His) or cpAaLS(Strep) fusion to LIX, cpAaLS(His)-tev*-LIX or cpAaLS(Strep)-tev*-LIX, respectively (Fig. 4a, single-component cage), since such a small peptide might not hinder cage assembly. For comparison, the peptide was also produced in fusion with His-tagged maltose-binding protein (MBP-LIX), frequently used as a fusion partner for microbial production of short peptides,[38] as well as with His-tag only (LIX). Those constructs were produced in *E. coli* cells and analyzed by SDS-PAGE using whole cells and soluble fractions after bacteriolysis (Fig. 4b, c and Fig. S6). While the His-tagged LIX was undetectable, substantial bands corresponding to the LIX fusion forms were observed for all other cases. The highest yield in the soluble fraction was obtained with the sole production of cpAaLS(His)-tev*-LIX, followed by its Strep-tagged variant cpAaLS(Strep)-tev*-LIX. These results suggested that the patchwork assembly approach is only necessary for bulky proteins and is not required for the small LIX peptide production within the AaLS cages. Furthermore, the encapsidic production seems superior to the conventional MBP-fusion strategy in terms of total production level and solubility. Considering the Strep-tagged cpAaLS showed a 15-fold higher purification yield than the His-tagged variant, we conclude that cpAaLS(Strep)-fusion is the best form among other tested constructs for producing LIX in *E. coli*.

Encapsidic production of other peptides with therapeutic potential

The general applicability of the encapsidic production system was investigated using five other peptides possessing

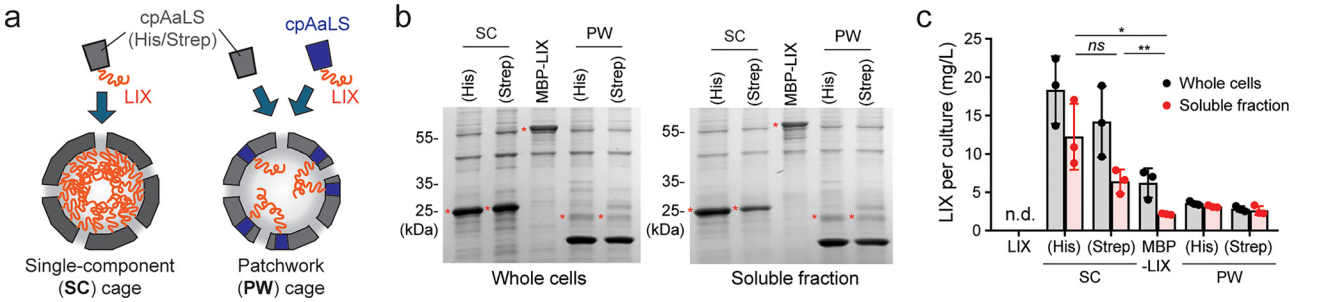

Fig. 4 Encapsidic production of lixisenatide. (a) Cartoon illustration of single component (SC) and patchwork (PW) cages containing lixisenatide (LIX). (b) and (c) SDS-PAGE analysis for LIX production using whole cells (left gel) and soluble fraction after bacteriolysis (right gel). The labels (His) or (Strep) indicate the purification tag of cpAaLS variants used for the single component (SC) or patchwork (PW) cages. LIX, LIX peptide alone; MBP-LIX, LIX fused to maltose-binding protein. The bands indicated with red asterisks were used for densitometry assay to estimate the LIX yield per liter of cell culture (c). Calculated molecular masses of proteins are; LIX, 6.6 kDa; cpAaLS(His)-LIX, 24.3 kDa; cpAaLS(Strep)-LIX, 24.6 kDa; MBP-LIX, 47.3 kDa; cpAaLS-LIX, 23.6 kDa. cpAaLS(His), 18.2 kDa; and cpAaLS(Strep), 18.5 kDa. Uncropped gel images, including BSA quantification standards, are also provided in Fig. S6. For panel c, data are shown as means ± standard deviation, along with the individual data points, from three biological replicates. n.d., not detected. ns – $p > 0.05$; * – $p < 0.1$; ** – $p < 0.01$ (student's *t*-test).

therapeutic potential: teriparatide (TER),[39] aviptadil (AVI),[40] thymosin β-4 (THY),[41] enfuvirtide (ENF),[42] and magainine-2 (MAG)[43] (Table S2). They were analogously produced as a fusion to cpAaLS(Strep) using *E. coli* cells and analyzed by SDS-PAGE. However, this showed that only THY was produced in a soluble form, and others almost exclusively ended up in insoluble fractions upon bacteriolysis (Fig. 5a, b and Fig. S7). In the case of MAG, substantial cytotoxicity was also observed, likely due to the bacteriolytic activity. These peptides that showed poor solubility with the encapsidic system are more hydrophobic than LIX and THY (Table S2), likely facilitating their aggregation and insolubility.

Reducing the fusion content of the protein cage using the patchwork assembly can overcome the solubility issues of the hydrophobic guests. These peptides were fused to cpAaLS and coproduced with cpAaLS(Strep). At 0.4 μg mL^{-1} tetracycline, nearly all the produced fusion protein was obtained in a soluble form for TER, AVI, and MAG, and ~60% for ENF (Fig. 5c and d). Unlike the single-component cage strategy with MAG, no remarkable cytotoxicity was observed for any peptides. Consequently, the patchwork approach increased the yield in the soluble fraction compared to the single-component cage by 1.8–5.5 fold (Fig. 5d, red filled *vs.* pink open circles). Induction

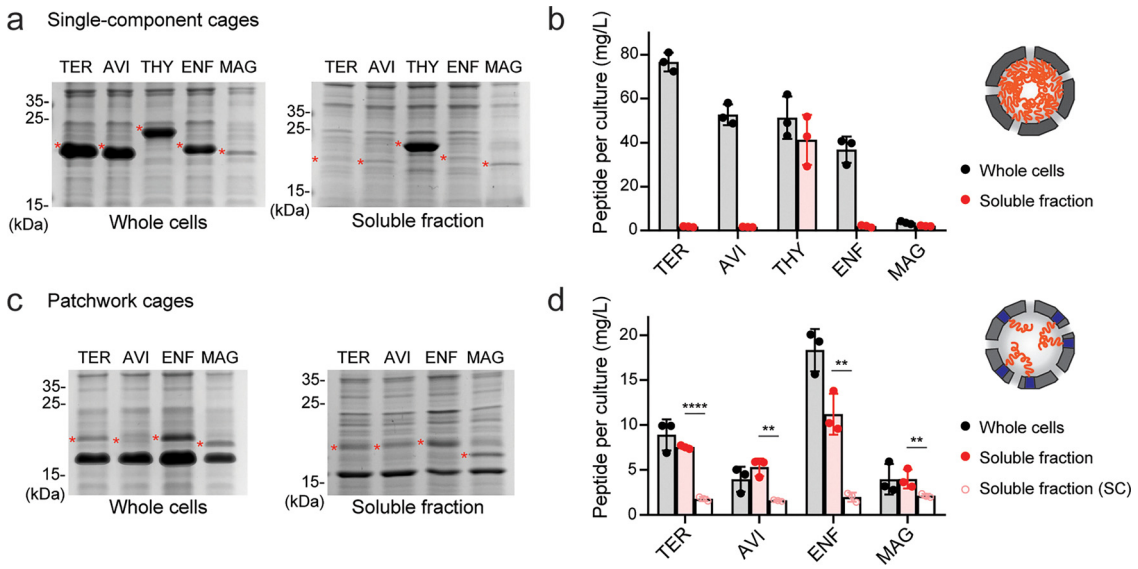

Fig. 5 Encapsidic production of therapeutic peptides. (a)–(d) SDS-PAGE analysis of peptides produced in single-component cages (a) and (b) or patchwork cages (c) and (d) using whole cells ((a) and (c), left gel) and soluble fraction after bacteriolysis ((a) and (c), right gel). The bands indicated with red asterisks were used for densitometry assay to estimate the yield per liter of cell culture (b) and (d). For panel d, the corresponding soluble fractions obtained in single-component cages (soluble fraction (SC), pink open circles), the same data as shown in panel b, are also provided for comparison. Calculated molecular masses of proteins are; cpAaLS(Strep)-TER, 24.0 kDa; cpAaLS(Strep)-AVI, 23.1 kDa; cpAaLS(Strep)-THY, 19.8 kDa; cpAaLS(Strep)-ENF, 24.2 kDa; cpAaLS(Strep)-MAG, 22.2 kDa; cpAaLS-TER, 22.8 kDa; cpAaLS-AVI, 22.0 kDa; cpAaLS-ENF, 23.1 kDa; and cpAaLS-MAG, 21.2 kDa. Uncropped gel images, including BSA quantification standard, are also provided in Fig. S7 and S8. For panels b and d, data are shown as means ± standard deviation, along with the individual data points, from three biological replicates. ** – $p < 0.01$; **** – $p < 0.0001$ (student's *t*-test).

with higher tetracycline concentration resulted in an increased proportion of the insoluble fraction for all the cases and no improvement in the protein yield in the soluble fraction (Fig. S8). Therefore, we conclude that optimization of guest density is crucial for producing hydrophobic peptides within protein cages in a soluble form. Furthermore, these results highlight that the patchwork assembly strategy is advantageous not only for intact cage formation with bulky protein cargo but also for solubilizing protein cages containing aggregation-prone peptides.

Isolation and characterization of encapsidically produced lixisenatide

After the successful encapsidic production of the LIX peptide, we tested the guest retrieval from the protein cages. Similarly to the GFP system, isolated cpAaLS(Strep)-tev*-LIX protein was treated with TEV protease. However, the cleavage was barely observed under a buffer condition used for GFP retrieval, 50 mM Tris–HCl buffer (pH 8.0) containing 0.3 M NaCl (Fig. 6a). Even though the cpAaLS(Strep) cages have pores, the high density of the guest peptide likely limits access of TEV protease to the lumen.

Efficient protease cleavage to release the LIX peptide from cpAaLS(Strep) was achieved by reduction in the NaCl concentration of the reaction buffer, *i.e.*, 50 mM Tris–HCl buffer (pH 8.5) without additional salt (Fig. 6a). This low ionic strength was previously found to disassemble cpAaLS cages into the pentameric subunits, where alkaline pH further facilitated the process.[22] This was also the case for the cpAaLS(Strep) variant (Fig. S2, right). While the TEM images of the isolated cpAaLS(Strep)-tev-LIX in 50 mM Tris–HCl (pH 8.0) buffer containing 0.3 M NaCl showed regular near-spherical structures with approximately 24-nm size (Fig. 6b, left), the same protein in 50 mM Tris–HCl buffer at pH 8.5 exhibited a similar size of particles but in uneven shapes (Fig. 6b, middle), likely reflecting partially broken shells. After the TEV protease cleavage reaction, they mostly disassembled into smaller fragments, and cage-like structures were not observed (Fig. 6b, right). The efficient cleavage was also observed in 50 mM Tris–HCl buffer at pH 7.5 and 8.0 without additional salt, but did not occur with 0.1–0.3 M NaCl regardless of pH (Fig. S9). Given the known minor impact of pH (6–9) and NaCl (0–2 M) on TEV protease catalytic activity,[44] the observed salt-dependent cleavage is most likely attributed to substrate accessibility. These results suggest that destabilization of cpAaLS(Strep) assembly by lowering ionic strength is crucial for retrieval of the cargo peptides by protease cleavage.

After the cleavage reaction, the sample containing LIX peptide was passed through Strep-Tactin affinity chromatography to remove cpAaLS(Strep) and the TEV protease, which also possesses a strep-tag. Subsequent purification using reverse-phase

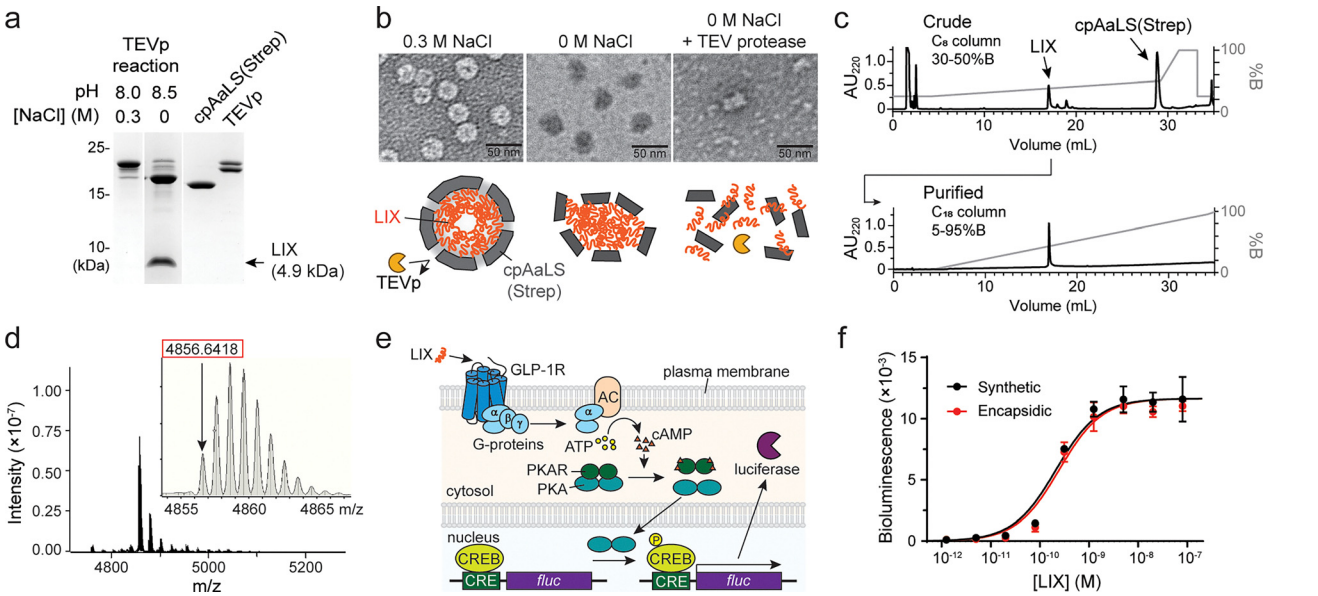

Fig. 6 LIX retrieval and characterization. (a) SDS-PAGE analysis of cpAaLS(Strep)-tev-LIX treated with TEV protease in 50 mM Tris–HCl buffer (pH 8.0 or 8.5) containing 0.3 or 0 M NaCl, respectively. The arrow indicates the band corresponding to LIX (4.9 kDa). The theoretical molecular masses of other proteins are as follows: cpAaLS(Strep)-tev-LIX, 24.6 kDa; cpAaLS(Strep), 18.5 kDa; and TEVp, 28.8 kDa. The corresponding uncropped gel image is provided in Fig. S9. (b) Negative-stain TEM images of cpAaLS(Strep)-tev-LIX in 50 mM Tris–HCl buffer (pH 8.0) containing 0.3 M NaCl (left) and in 50 mM Tris–HCl buffer (pH 8.5) before (middle) and after (right) TEV protease treatment. A possible mechanism of TEV protease access to the guest peptide is shown below the micrographs. (c) Reverse-phase high-performance liquid chromatography (RP-HPLC) analysis of crude (top) and purified LIX (bottom). (d) Mass spectrometry of purified LIX. The enlarged view of the main peak is shown in the inset. The theoretical monoisotopic mass of LIX is 4856.53. (e) Diagram of the glucagon-like peptide-1 receptor (GLP-1R)-mediated reporter assay system. AC, adenylyl cyclase; PKA, protein kinase A; PKAR, PKA regulator; CRE, cAMP-response element; CREB, CRE-binding protein; fluc, firefly luciferase; and P, phosphate group. (f) The activity of LIX on the stimulation of GLP-1R. Data using a commercially available synthetic standard (black) are provided as a reference for the encapsidically produced and isolated LIX (red). Data are shown as means ± standard deviation from triplicate measurements. EC_{50} values of synthetic and encapsidically produced LIX were determined to be 0.28 ± 0.09 and 0.35 ± 0.15 nM, respectively.

high-performance liquid chromatography (RP-HPLC) yielded the LIX peptide with ~100% purity (Fig. 6c). The fidelity of the purified LIX was confirmed by electrospray ionization mass spectrometry (ESI-MS), observing 4856.64 (theoretical mass: 4856.53) (Fig. 6d and Fig. S10). Approximately 0.3 mg of LIX was obtained from an *E. coli* cell culture in a 0.5-L LB medium.

The activity of the encapsidically produced LIX peptide was tested using a genetically engineered human embryonic kidney (HEK) cell line that produces human GLP-1 receptor (GLP-1R) (Fig. S11) and carries a firefly luciferase reporter under the control of cyclic adenosine monophosphate (cAMP) response element (CRE) (Fig. 6e). The binding of LIX to the GLP-1R should trigger the activation of coupled G-proteins, leading to an increase in intracellular concentrations of cAMP. Bioluminescence of luciferase, of which the gene expression is induced by cAMP, was used as a readout of the successful stimulation of the GLP-1R. The encapsidically produced LIX peptide showed GLP-1R stimulation activity comparable to a synthetic standard of the same peptide (Fig. 6f). These results exemplify that the encapsidic production can be utilized for a functional therapeutic peptide.

Conclusions

The subcellular compartmentalization using an engineered protein cage establishes a practical means for microbial production and isolation of degradation-prone polypeptides. Genetic fusion to a cage-component protein ensures efficient compartmentalization of cargo peptides, protecting them from cellular proteolytic machinery. Besides proteolysis focused here, spatial segregation by protein shells potentially circumvents other problems encountered during heterologous protein production. For instance, cytotoxicity of a membrane-disrupting antimicrobial peptide MAG can be suppressed by encapsulation in AaLS protein cages (Fig. 5),[43] while a similar attenuation effect has also been shown for a toxic protease from human immunodeficiency virus (HIV).[45] Protein shells may also prevent the entry of undesired cellular enzymes, such as reductases that cleave disulfide bonds and destabilize protein folding.[46] The patchwork assembly system is advantageous for these purposes, as it allows customizing the morphology and chemical properties of protein cages for individual cargo by selecting an appropriate variant as a scaffolding protein.[20] For example, protein cages formed by negatively supercharged AaLS variants can be utilized to exclude unwanted polyanionic molecules.[47] This modularity makes the AaLS-based system a potent technology for producing a variety of difficult-to-express proteins.

To date, substantial efforts have been directed towards the efficient microbial production of short peptides as an ecological and economical alternative to canonical chemical synthesis. As shown with MBP for LIX (Fig. 4b), fusion to a soluble protein can reduce the degradation and cytotoxicity, the most common issues during recombinant peptide production.[38] However, this approach still exposes peptides, leaving a chance for proteolysis during production and purification. An alternative strategy is based on the targeting of peptides to inclusion bodies that also segregate the products from other cellular contents.[48] Meanwhile, retrieval of aggregation-prone peptides from the inclusion body often requires harsh chemical conditions, including high concentrations of chaotropic agents, which limit the usage of enzymes for downstream processes, *e.g.*, sequence-specific cleavage. Protein cages that solubilize and segregate cargo peptides until exposing them by lowering ionic strength provide an ideal scenario, enabling both protection within cells and further enzymatic processing of peptides.

Therapeutic peptide production within protein cages is potentially useful for drug discovery and delivery. This genetically encoded peptide biosynthesis can facilitate their mutagenesis and evolutionary engineering toward improved biological activity, *e.g.*, higher affinity to target receptors. As shown for lixisenatide, affinity chromatography followed by protease cleavage yielded a desired peptide with purity likely sufficient for screening purposes (Fig. 5c). Furthermore, protein cages that apparently enlarge and shield cargo molecules may improve otherwise limited bioavailability of peptide therapeutics that are, in general, rapidly eliminated by renal filtration and degraded by proteases because of their small and flexible structural characteristics.[35] On the other hand, the cargo release, which relies on lowering ionic strength and a plant-virus-derived protease, is most likely unsuitable for direct *in vivo* application. Toward the development of more versatile, smart nanocarriers, further reengineering of the AaLS protein to induce cage disassembly and cargo release by a defined, biocompatible stimulus relevant to disease environment is ongoing in our laboratory.

Author contributions

A. G., J. P., M. Z., D. Kw., D. Kl, and Y. A. performed experiments and analyzed data. Y. A. conceptualized the project, oversaw the research, acquired the funding, prepared the figures, and wrote the original draft. A. G., J. P., M. Z., D. Kw., L. K., S. G., N. KT., and Y. A. reviewed and edited the manuscript. All the authors contributed to the experimental design, as well as read and approved the final version of the manuscript.

Conflicts of interest

There are no conflicts to declare.

Data availability

All experimental supporting data and procedures are available in the SI.[49,50] See DOI: **https://doi.org/10.1039/d5tb01033k**.

Acknowledgements

We would like to thank Dr Michał Bochenek (Malopolska Centre of Biotechnology (MCB), Jagiellonian University (JU), Krakow) for his help with the flow cytometry experiments, Dr Urszula Jankowska and Dr Bożena Skupień-Rabian (MCB, JU) with mass spectrometry, as well as Dr Olga Woźnicka and Dr Elżbieta Pyza (Faculty of Biology, JU) with negative-stain

transmission electron microscopy. This work was generously supported by National Science Centre of Poland (NCN) grants (Opus-18, 2019/35/B/NZ1/02044) and an EMBO Installation Grant. D.Kw is grateful for a European Research Area (ERA) fellowship. The open-access publication of this article was funded by the Priority Research Area BioS under the program 'Initiative of Excellence – Research University' at JU.

References

1 K. Škubník, L. Sukeník, D. Buchta, T. Füzik, M. Procházková, J. Moravcová, L. Šmerdová, A. Přidal, R. Vácha and P. Plevka, Capsid opening enables genome release of iflaviruses, *Sci. Adv.*, 2021, **7**, eabd7130.

2 J. E. Eschbach, J. L. Elliott, W. Li, K. K. Zadrozny, K. Davis, S. J. Mohammed, D. Q. Lawson, O. Pornillos, A. N. Engelman and S. B. Kutluay, Capsid lattice destabilization leads to premature loss of the viral genome and integrase enzyme during HIV-1 infection, *J. Virol.*, 2020, **95**, DOI: **10.1128/jvi.00984-20**.

3 K. R. Harrison, D. Snead, A. Kilts, M. L. Ammerman and K. R. Wigginton, The protective effect of virus capsids on RNA and DNA virus genomes in wastewater, *Environ. Sci. Technol.*, 2023, **57**, 13757–13766.

4 D. He and J. Marles-Wright, Ferritin family proteins and their use in bionanotechnology, *New Biotechnol.*, 2015, **32**, 651–657.

5 W. M. Aumiller, M. Uchida and T. Douglas, Protein cage assembly across multiple length scales, *Chem. Soc. Rev.*, 2018, **47**, 3433–3469.

6 T. G. W. Edwardson, M. D. Levasseur, S. Tetter, A. Steinauer, M. Hori and D. Hilvert, Protein cages: from fundamentals to advanced applications, *Chem. Rev.*, 2022, **122**, 9145–9197.

7 E. J. Lee, N. K. Lee and I. S. Kim, Bioengineered protein-based nanocage for drug delivery, *Adv. Drug Delivery Rev.*, 2016, **106**, 157–171.

8 Y. Azuma, T. G. W. Edwardson, N. Terasaka and D. Hilvert, Modular protein cages for size-selective RNA packaging in vivo, *J. Am. Chem. Soc.*, 2018, **140**, 566–569.

9 N. Terasaka, Y. Azuma and D. Hilvert, Laboratory evolution of virus-like nucleocapsids from nonviral protein cages, *Proc. Natl. Acad. Sci. U. S. A.*, 2018, **115**, 5432.

10 S. Tetter, N. Terasaka, A. Steinauer, R. J. Bingham, S. Clark, A. J. P. Scott, N. Patel, M. Leibundgut, E. Wroblewski, N. Ban, P. G. Stockley, R. Twarock and D. Hilvert, Evolution of a virus-like architecture and packaging mechanism in a repurposed bacterial protein, *Science*, 2021, **372**, 1220–1224.

11 P.-Y. Fang, J. C. Bowman, L. M. Gómez Ramos, C. Hsiao and L. D. Williams, RNA: packaged and protected by VLPs, *RSC Adv.*, 2018, **8**, 21399–21406.

12 A. Raguram, M. An, P. Z. Chen and D. R. Liu, Directed evolution of engineered virus-like particles with improved production and transduction efficiencies, *Nat. Biotechnol.*, 2024, DOI: **10.1038/s41587-024-02467-x**.

13 E. Y. Kim and D. Tullman-Ercek, A rapid flow cytometry assay for the relative quantification of protein encapsulation into bacterial microcompartments, *Biotechnol. J.*, 2014, **9**, 348–354.

14 C. M. Jakobson, E. Y. Kim, M. F. Slininger, A. Chien and D. Tullman-Ercek, Localization of proteins to the 1,2-propanediol utilization microcompartment by non-native signal sequences is mediated by a common hydrophobic motif, *J. Biol. Chem.*, 2015, **290**, 24519–24533.

15 M. J. Lee, I. R. Brown, R. Juodeikis, S. Frank and M. J. Warren, Employing bacterial microcompartment technology to engineer a shell-free enzyme-aggregate for enhanced 1,2-propanediol production in Escherichia coli, *Metab. Eng.*, 2016, **36**, 48–56.

16 Y. H. Lau, T. W. Giessen, W. J. Altenburg and P. A. Silver, Prokaryotic nanocompartments form synthetic organelles in a eukaryote, *Nat. Commun.*, 2018, **9**, 1311.

17 F. Sigmund, C. Massner, P. Erdmann, A. Stelzl, H. Rolbieski, M. Desai, S. Bricault, T. P. Wörner, J. Snijder, A. Geerlof, H. Fuchs, M. Hrabe de Angelis, A. J. R. Heck, A. Jasanoff, V. Ntziachristos, J. Plitzko and G. G. Westmeyer, Bacterial encapsulins as orthogonal compartments for mammalian cell engineering, *Nat. Commun.*, 2018, **9**, 1990.

18 L. C. Cheah, T. Stark, L. S. R. Adamson, R. S. Abidin, Y. H. Lau, F. Sainsbury and C. E. Vickers, Artificial self-assembling nanocompartment for organizing metabolic pathways in yeast, *ACS Synth. Biol.*, 2021, **10**, 3251–3263.

19 D. Zakaszewski, L. Koziej, J. Pankowski, V. V. Malolan, N. Gämperli, J. G. Heddle, D. Hilvert and Y. Azuma, Complementary charge-driven encapsulation of functional protein by engineered protein cages in cellulo, *J. Mater. Chem. B*, 2023, **11**, 6540–6546.

20 Y. Azuma, M. Herger and D. Hilvert, Diversification of protein cage structure using circularly permuted subunits, *J. Am. Chem. Soc.*, 2018, **140**, 558–561.

21 E. Sasaki, D. Böhringer, M. van de Waterbeemd, M. Leibundgut, R. Zschoche, A. J. Heck, N. Ban and D. Hilvert, Structure and assembly of scalable porous protein cages, *Nat. Commun.*, 2017, **8**, 14663.

22 L. Koziej, F. Fatehi, M. Aleksejczuk, M. J. Byrne, J. G. Heddle, R. Twarock and Y. Azuma, Dynamic assembly of pentamer-based protein nanotubes, *ACS Nano*, 2025, **19**, 8786–8798.

23 Y. Azuma, T. G. W. Edwardson and D. Hilvert, Tailoring lumazine synthase assemblies for bionanotechnology, *Chem. Soc. Rev.*, 2018, **47**, 3543–3557.

24 X. Zhang, W. Meining, M. Fischer, A. Bacher and R. Ladenstein, X-ray structure analysis and crystallographic refinement of lumazine synthase from the hyperthermophile Aquifex aeolicus at 1.6 A resolution: determinants of thermostability revealed from structural comparisons, *J. Mol. Biol.*, 2001, **306**, 1099–1114.

25 G.-F. Tu, G. E. Reid, J.-G. Zhang, R. L. Moritz and R. J. Simpson, C-terminal extension of truncated recombinant proteins in Escherichia coli with a 10Sa RNA decapeptide, *J. Biol. Chem.*, 1995, **270**, 9322–9326.

26 M. Lies and M. R. Maurizi, Turnover of endogenous SsrA-tagged proteins mediated by ATP-dependent proteases in Escherichia coli, *J. Biol. Chem.*, 2008, **283**, 22918–22929.

27 Y. Azuma, R. Zschoche, M. Tinzl and D. Hilvert, Quantitative packaging of active enzymes into a protein cage, *Angew. Chem., Int. Ed.*, 2016, **55**, 1531–1534.
28 C. E. Correnti, M. M. Gewe, C. Mehlin, A. D. Bandaranayake, W. A. Johnsen, P. B. Rupert, M.-Y. Brusniak, M. Clarke, S. E. Burke, W. De Van Der Schueren, K. Pilat, S. M. Turnbaugh, D. May, A. Watson, M. K. Chan, C. D. Bahl, J. M. Olson and R. K. Strong, Screening, large-scale production and structure-based classification of cystine-dense peptides, *Nat. Struct. Mol. Biol.*, 2018, **25**, 270–278.
29 R. B. Kapust, J. Tözsér, J. D. Fox, D. E. Anderson, S. Cherry, T. D. Copeland and D. S. Waugh, Tobacco etch virus protease: mechanism of autolysis and rational design of stable mutants with wild-type catalytic proficiency, *Protein Eng., Des. Sel.*, 2001, **14**, 993–1000.
30 L. D. Cabrita, D. Gilis, A. L. Robertson, Y. Dehouck, M. Rooman and S. P. Bottomley, Enhancing the stability and solubility of TEV protease using in silico design, *Protein Sci.*, 2007, **16**, 2360–2367.
31 E. Gur, D. Biran and E. Z. Ron, Regulated proteolysis in Gram-negative bacteria – how and when?, *Nat. Rev. Microbiol.*, 2011, **9**, 839–848.
32 Q. Zhao, W. Xu, L. Xing and Z. Lin, Recombinant production of medium- to large-sized peptides in Escherichia coli using a cleavable self-aggregating tag, *Microb. Cell Fact.*, 2016, **15**, 136.
33 N. Goda, N. Matsuo, T. Tenno, S. Ishino, Y. Ishino, S. Fukuchi, M. Ota and H. Hiroaki, An optimized Nprobased method for the expression and purification of intrinsically disordered proteins for an NMR study, *Intrinsically Disord. Proteins*, 2015, **3**, e1011004.
34 L. Ferrazzano, M. Catani, A. Cavazzini, G. Martelli, D. Corbisiero, P. Cantelmi, T. Fantoni, A. Mattellone, C. De Luca, S. Felletti, W. Cabri and A. Tolomelli, Sustainability in peptide chemistry: current synthesis and purification technologies and future challenges, *Green Chem.*, 2022, **24**, 975–1020.
35 L. Wang, N. Wang, W. Zhang, X. Cheng, Z. Yan, G. Shao, X. Wang, R. Wang and C. Fu, Therapeutic peptides: current applications and future directions, *Signal Transduction Targeted Ther.*, 2022, **7**, 48.
36 M. Muttenthaler, G. F. King, D. J. Adams and P. F. Alewood, Trends in peptide drug discovery, *Nat. Rev. Drug Discovery*, 2021, **20**, 309–325.
37 U. Werner, G. Haschke, A. W. Herling and W. Kramer, Pharmacological profile of lixisenatide: A new GLP-1 receptor agonist for the treatment of type 2 diabetes, *Regul. Pept.*, 2010, **164**, 58–64.
38 L. Gardijan, M. Miljkovic, M. Obradovic, B. Borovic, G. Vukotic, G. Jovanovic and M. Kojic, Redesigned pMAL expression vector for easy and fast purification of active native antimicrobial peptides, *J. Appl. Microbiol.*, 2022, **133**, 1001–1013.
39 R. M. Neer, C. D. Arnaud, J. R. Zanchetta, R. Prince, G. A. Gaich, J.-Y. Reginster, A. B. Hodsman, E. F. Eriksen, S. Ish-Shalom, H. K. Genant, O. Wang, D. Mellström, E. S. Oefjord, E. Marcinowska-Suchowierska, J. Salmi, H. Mulder, J. Halse, A. Z. Sawicki and B. H. Mitlak, Effect of parathyroid hormone (1-34) on fractures and bone mineral density in postmenopausal women with osteoporosis, *N. Engl. J. Med.*, 2001, **344**, 1434–1441.
40 V. Petkov, W. Mosgoeller, R. Ziesche, M. Raderer, L. Stiebellehner, K. Vonbank, G.-C. Funk, G. Hamilton, C. Novotny, B. Burian and L.-H. Block, Vasoactive intestinal peptide as a new drug for treatment of primary pulmonary hypertension, *J. Clin. Invest.*, 2003, **111**, 1339–1346.
41 A. L. Goldstein, E. Hannappel and H. K. Kleinman, Thymosin β4: actin-sequestering protein moonlights to repair injured tissues, *Trends Mol. Med.*, 2005, **11**, 421–429.
42 J. M. Kilby, J. P. Lalezari, J. J. Eron, M. Carlson, C. Cohen, R. C. Arduino, J. C. Goodgame, J. E. Gallant, P. Volberding, R. L. Murphy, F. Valentine, M. S. Saag, E. L. Nelson, P. R. Sista and A. Dusek, The safety, plasma pharmacokinetics, and antiviral activity of subcutaneous Enfuvirtide (T-20), a peptide inhibitor of gp41-mediated virus fusion, in HIV-infected adults, *AIDS Res. Hum. Retroviruses*, 2002, **18**, 685–693.
43 M. Zasloff, Magainins, a class of antimicrobial peptides from Xenopus skin: isolation, characterization of two active forms, and partial cDNA sequence of a precursor, *Proc. Natl. Acad. Sci. U. S. A.*, 1987, **84**, 5449–5453.
44 T. D. Parks, E. D. Howard, T. J. Wolpert, D. J. Arp and W. G. Dougherty, Expression and Purification of a Recombinant Tobacco Etch Virus NIa Proteinase: Biochemical Analyses of the Full-Length and a Naturally Occurring Truncated Proteinase Form, *Virology*, 1995, **210**, 194–201.
45 B. Wörsdörfer, K. J. Woycechowsky and D. Hilvert, Directed evolution of a protein container, *Science*, 2011, **331**, 589–592.
46 P. H. Bessette, F. Åslund, J. Beckwith and G. Georgiou, Efficient folding of proteins with multiple disulfide bonds in the Escherichia coli cytoplasm, *Proc. Natl. Acad. Sci. U. S. A.*, 1999, **96**, 13703–13708.
47 Y. Azuma, D. L. V. Bader and D. Hilvert, Substrate sorting by a supercharged nanoreactor, *J. Am. Chem. Soc.*, 2018, **140**, 860–863.
48 P. M. Hwang, J. S. Pan and B. D. Sykes, Targeted expression, purification, and cleavage of fusion proteins from inclusion bodies in Escherichia coli, *FEBS Lett.*, 2014, **588**, 247–252.
49 Y. Azuma, R. Zschoche and D. Hilvert, The C-terminal peptide of Aquifex aeolicus riboflavin synthase directs encapsulation of native and foreign guests by a cage-forming lumazine synthase, *J. Biol. Chem.*, 2017, **292**, 10321–10327.
50 Y. Azuma, S. Gaweł, M. Pasternak, O. Woźnicka, E. Pyza and J. G. Heddle, Reengineering of an artificial protein cage for efficient packaging of active enzymes, *Small*, 2024, **20**, 2312286.